CrossMark

ORIGINAL ARTICLE

Isolation of novel PSII-LHCII megacomplexes from pea plants characterized by a combination of proteomics and electron microscopy

Pascal Albanese[1,2] · Jon Nield[3] · Jose Alejandro Muñoz Tabares[4] ·
Angelica Chiodoni[4] · Marcello Manfredi[5,6] · Fabio Gosetti[6] · Emilio Marengo[6] ·
Guido Saracco[1] · James Barber[7] · Cristina Pagliano[1]

Abstract In higher plants, photosystem II (PSII) is a multi-subunit pigment-protein complex embedded in the thylakoid membranes of chloroplasts, where it is present mostly in dimeric form within the grana. Its light-harvesting antenna system, LHCII, is composed of trimeric and monomeric complexes, which can associate in variable number with the dimeric PSII core complex in order to form different types of PSII-LHCII supercomplexes. Moreover, PSII-LHCII supercomplexes can laterally associate within the thylakoid membrane plane, thus forming higher molecular mass complexes, termed PSII-LHCII megacomplexes (Boekema et al. 1999a, in Biochemistry 38:2233–2239; Boekema et al. 1999b, in Eur J Biochem 266:444–452). In this study, pure PSII-LHCII megacomplexes were directly isolated from stacked pea thylakoid membranes by a rapid single-step solubilization, using the detergent n-dodecyl-α-D-maltoside, followed by sucrose gradient ultracentrifugation. The megacomplexes were subjected to biochemical and structural analyses. Transmission electron microscopy on negatively stained samples, followed by single-particle analyses, revealed a novel form of PSII-LHCII megacomplexes, as compared to previous studies (Boekema et al.1999a, in Biochemistry 38:2233–2239; Boekema et al. 1999b, in Eur J Biochem 266:444–452), consisting of two PSII-LHCII supercomplexes sitting side-by-side in the membrane plane, sandwiched together with a second copy. This second copy of the megacomplex is most likely derived from the opposite membrane of a granal stack. Two predominant forms of intact sandwiched megacomplexes were observed and termed, according to (Dekker and Boekema 2005 Biochim Biophys Acta 1706:12–39), as $(C_2S_2)_4$ and $(C_2S_2 + C_2S_2\text{-}M_2)_2$ megacomplexes. By applying a gel-based proteomic approach, the protein composition of the isolated megacomplexes was fully characterized. In summary, the new structural forms of isolated megacomplexes and the related modeling performed provide novel insights into how PSII-LHCII supercomplexes may bind to each other, not only in the membrane plane, but also between granal stacks within the chloroplast.

Abbreviations

ATP-ase	ATP-synthase

✉ Cristina Pagliano
cristina.pagliano@polito.it

1 Applied Science and Technology Department - BioSolar Lab, Politecnico di Torino, Viale T. Michel 5, 15121 Alessandria, Italy

2 Department of Biology, University of Padova, Via Ugo Bassi 58 B, 35121 Padova, Italy

3 School of Biological and Chemical Sciences, Queen Mary University of London, London E1 4NS, UK

4 Center for Space Human Robotics IIT@POLITO, Istituto Italiano di Tecnologia, Corso Trento 21, 10129 Turin, Italy

5 ISALIT–Department of Science and Technological Innovation, University of Eastern Piedmont, Viale T. Michel 11, 15121 Alessandria, Italy

6 Department of Science and Technological Innovation, University of Eastern Piedmont, Viale T. Michel 11, 15121 Alessandria, Italy

7 Department of Life Sciences, Faculty of Natural Sciences, Imperial College London, London SW7 2AZ, UK

Chl	Chlorophyll
Cyt	Cytochrome
2D	Two-dimensional
3D	Three-dimensional
α-DDM	n-Dodecyl-α-D-maltoside
HPLC	High-performance liquid chromatography
LHC	Light-harvesting complex
lpBN-PAGE	Large-pore blue native polyacrylamide gel electrophoresis
MS	Mass spectrometry
OEC	Oxygen-evolving complex
PS	Photosystem
RC	Reaction center
SDS-PAGE	Sodium dodecyl sulfate polyacrylamide gel electrophoresis
TEM	Transmission electron microscopy

Introduction

The thylakoid membranes of higher plants form a highly plastic and dynamic membrane system characterized by a peculiar feature, the presence of granal stacks, or grana (Nevo et al. 2009). Tight granal stacking is typically observed, with two grana membrane pairs being separated by ∼3.5 nm on the stromal side and with a lumenal width of 4.5 nm (Daum et al. 2010; Kirchhoff et al. 2011). A consequence of grana formation is the structural sub-compartmentalization of the thylakoid membrane system into tightly stacked and exposed unstacked regions, and the subsequent lateral distribution of protein complexes between these sub-compartments. Photosystem I (PSI) (Amunts and Nelson 2009) and ATP-synthase (ATP-ase) (Groth and Pohl 2001) have bulky stromal protrusions and, mainly due to this, are confined to unstacked stroma lamellae and the granal margins, whereas Photosystem II (PSII) and its light-harvesting complex (LHCII), with their relatively flat stromal surfaces, are concentrated in the grana membranes (Andersson and Anderson 1980; Albertsson 2001). It is widely believed that interactions between the stromal protein moieties of LHCIIs, localized in adjacent-stacked membranes, are one of the main determinants for grana formation (Mullet 1983), although surface electrical charge properties play an important role (Barber 1982).

PSII is a multi-subunit pigment-protein complex that normally functions as a dimer within the grana of higher plants (Hankamer et al. 1997). Within the dimer, each of the two monomeric cores contains the integral subunits D1 and D2. These proteins bind most of the redox cofactors required to propagate the photosynthetic electron transport chain and, together with the α and β subunits of cytochrome b559 (Cyt b559) and the low molecular subunit PsbI, constitute the reaction center (RC) of PSII, a term used in this case to define the minimum unit for sustaining primary charge separation (Nanba and Satoh 1987). The RC proteins are closely associated with the two inner antenna proteins CP47 and CP43 and bind additional low molecular mass membrane subunits, which play a key role in the assembly and stabilization of the overall PSII core complex (for details see the recent review Pagliano et al. 2013). This core complex, to be fully functional, requires the assembly of the oxygen-evolving complex (OEC), containing the Mn_4CaO_5 cluster which, in higher plants, is stabilized by the extrinsic subunits PsbO, PsbP, PsbQ and PsbR. Up to now, the most highly resolved three-dimensional (3D) structure available for the plant PSII core complex has been obtained by electron crystallography at 8 Å, allowing for the position and helix organization of the major subunits to be revealed (Rhee et al. 1998; Hankamer et al. 2001). Moreover, crystal structures have been determined for the isolated extrinsic polypeptides PsbP (Ifuku et al. 2004) and PsbQ (Calderone et al. 2003; Balsera et al. 2005). In higher plants, the dimeric PSII RC core is serviced by a variable number of intrinsic light-harvesting proteins, named Lhcb1–6, binding chlorophyll (Chl) a and Chl b. The Lhcb1-3 subunits typically occur in a ratio of about 8:3:1 (Jansson 1994; Jackowski et al. 2001; Caffarri et al. 2004) and form several types of major LHCII homo- and hetero-trimers, whose high-resolution structures have been solved by X-ray crystallography (Liu et al. 2004; Standfuss et al. 2005). They interact specifically with the PSII core via the minor LHCII monomeric antenna proteins Lhcb4, Lhcb5, and Lhcb6. So far, among these minor LHCII antenna proteins, an atomically resolved 3D structure is available only for Lhcb4 (Pan et al. 2011).

A variable number of LHCII proteins can associate with the dimeric PSII core complex to form different types of PSII-LHCII supercomplexes, named according to their composition (Dekker and Boekema 2005). In terms of nomenclature, the so-called C_2S_2 supercomplex, whose 3D structure at the highest resolution has been obtained at 17 Å from spinach by single-particle cryo-transmission electron microscopy (cryo-TEM) (Nield et al. 2000; Nield and Barber 2006), consists of a dimeric PSII core complex (C_2) that binds to two LHCII trimers in a relatively strong way (i.e., S-trimers) via two copies of the monomeric Lhcb4 and Lhcb5 subunits. Larger PSII-LHCII supercomplexes, containing two extra copies of the monomeric Lhcb6 with one or two additional LHCII trimers, moderately bound to the dimeric PSII core complex (i.e., M-trimers) via Lhcb4 and Lhcb6, are known as $C_2S_2M_{1-2}$ (Dekker and Boekema 2005). For the $C_2S_2M_2$ supercomplex, 2D projection maps and a low resolution (30 Å) 3D model have been obtained

by TEM and single-particle analysis of negatively stained particles isolated, respectively, from *Arabidopsis* (Yakushevska et al. 2001; Caffarri et al. 2009) and pea plants (Pagliano et al. 2014). Occasionally, but only in membranes partially solubilized with detergents, larger supercomplexes have been observed by TEM, with one or two additional LHCII trimers (i.e., L-trimers) even more loosely bound to the dimeric PSII core complex, via Lhcb6, known as $C_2S_2M_{0-2}L_{1-2}$ (Boekema et al. 1999a). Using TEM and image analysis on negatively stained BBY membranes isolated from spinach, only partially solubilized with the mild detergent n-dodecyl-α-D-maltoside (α-DDM), Boekema and colleagues observed even larger complexes, termed megacomplexes, identified as dimeric associations of PSII-LHCII supercomplexes interacting with each other, within the membrane, in three different binding sites (Boekema et al. 1999a, b). The type I megacomplex ($C_4S_4M_{2-4}$), with a square-like shape, and type II megacomplex ($C_4S_4M_{2-4}$), with a rectangular-like shape, consist of two C_2S_2M supercomplexes arranged in an antiparallel fashion with a translational shift of about 7.5 nm for one of the C_2S_2M units (Boekema et al. 1999a); type III megacomplex (C_4S_4), with a windmill-like shape, is made up of two C_2S_2 supercomplexes connected at their Lhcb5 tips (Boekema et al. 1999b).

In this study, PSII-LHCII megacomplexes were isolated by a quick, single-step, solubilization using α-DDM on stacked thylakoid membranes extracted from pea plants, and their structures have been analyzed by TEM and subsequent image analysis of negatively stained single particles at a resolution of ~18 Å. This structural study was integrated with biochemical information, obtained by applying a gel-based proteomic approach to the isolated PSII-LHCII megacomplexes, to analyze their protein composition. Overall, these data indicate that screening for the native association of membrane protein complexes by single-particle TEM and mass spectrometry is a valuable approach to fully characterize large megacomplexes and their supramolecular organization within the granal membranes of higher plant chloroplasts.

Materials and methods

Isolation of PSII-LHCII megacomplexes

Pea plants were grown for 3 weeks under 8 h daylight at 20 °C, 60 % humidity, and 150 µmol m^{-2} s^{-1} photons (conditions provided by the growth chamber SANYO MLR-351H with 15 Fluorescent lamps, of 40 W each, switched on). Stacked thylakoid membranes were isolated from plants at the end of the daily dark phase of growth as described in detail earlier (Pagliano et al. 2012). Briefly,

stacked thylakoid membranes, at a Chl concentration of 1 mg mL^{-1}, were treated with 50 mM α-DDM for 1 min at 4 °C in the dark according to Barera et al. (2012). Phenylmethylsulphonylfluoride (500 µM) was present during the solubilization to inhibit protease activity. After centrifugation, at 21,000×g for 10 min at 4 °C, 700 µL of supernatant was added to the top of a linear sucrose gradient, previously prepared by a freezing and thawing cycle applied to ultracentrifuge tubes filled with a buffer made of 0.65 M sucrose, 25 mM MES pH 5.7, 10 mM NaCl, 5 mM CaCl$_2$, and 0.03 % (w/v) α-DDM. Centrifugation was carried out at 100,000 g for 12 h at 4 °C (Surespin 630 rotor, Thermo Scientific).

The sucrose band containing PSII-LHCII megacomplexes was carefully harvested using a syringe and, if necessary, concentrated by membrane filtration via Amicon Ultra 100 kDa cut-off devices (Millipore) and then flash frozen for storage at −80 °C.

Spectroscopic analyses

The Chl concentration was determined spectrophotometrically after extraction in 80 % (v/v) acetone according to (Arnon 1949). Absorption spectra in native conditions were recorded using a Lambda25 spectrophotometer (Perkin Elmer) at 12 °C. Low-temperature (77 K) fluorescence emission spectra were registered by a FL55 spectrofluorometer (Perkin Elmer), equipped with a red-sensitive photomultiplier and a low-temperature cuvette holder. Samples were excited at 436 nm. The spectral bandwidths were 7.5 nm (excitation) and 3 nm (emission). The Chl concentration was approximately 0.5 µg mL^{-1} in 90 % (v/v) glycerol and 10 % (v/v) sucrose gradient buffer.

Gel electrophoresis

Optimal separation of the thylakoid membrane protein complexes and PSII-LHCII megacomplexes was obtained as in Järvi et al. (2011), using large-pore blue native polyacrylamide gel electrophoresis (lpBN-PAGE) on gels 20 cm × 16 cm, containing an acrylamide gradient of 3-12 % (w/v) T and 3.33 % (w/v) C in the resolving gel, and 3 % (w/v) T and 20 % (w/v) C in the stacking gel. Either solubilized pea thylakoids or the band from the sucrose density gradient were mixed to a final Chl concentration of 300 µg mL^{-1} with BN-loading buffer (5 % (w/v) Coomassie Blue G250, 750 mM ε-amino caproic acid) at a volume ratio of 16:1. After incubation for 10 min on ice and a brief centrifugation at 20,000×g for 10 min, the subsequent supernatants were loaded onto the gel. Electrophoresis was performed at a constant voltage of 70 V at 9 °C for 20 h. The anode buffer was made of 50 mM Bis–Tris-HCl pH 7.0, the cathode buffer of 50 mM

Tricine, 15 mM Bis–Tris-HCl pH 7.0, and 0.02 % (w/v) Coomassie G250; the latter being replaced, after two-thirds of the run, by a cathode buffer with the same composition but devoid of Coomassie G250. For molecular mass markers, a mixture of lyophilized standard proteins (Amersham, high molecular weight calibration kit code 17-0445-01, GE Healthcare) and blue dextran (code D575, Sigma-Aldrich) was used.

For two-dimensional sodium dodecyl sulfate polyacrylamide gel electrophoresis (2D SDS-PAGE), lanes from the lpBN-PAGE were excised and denatured in 66 mM Na_2 CO_3, 0.66 % (v/v) β-mercaptoethanol and 2 % (w/v) SDS at room temperature for 40 min. After denaturation, proteins were resolved by SDS-PAGE according to the Laemmli's system (Laemmli 1970) on a 15 % (w/v) polyacrylamide gel containing 6 M urea. Electrophoresis was carried out at a constant amperage of 10 mA for 17 h at 9 °C. Gels were stained using a mass spectrometry compatible silver staining protocol as described in Shevchenko et al. (1996).

2D SDS-PAGE and/or mono-dimensional SDS-PAGE, the latter being performed on a 12.5 % (w/v) polyacrylamide gel containing 5 M urea using Laemmli's system (Laemmli 1970), were transferred onto nitro-cellulose membranes and further immunodetected with specific antisera against PsbO, PsbP, PsbQ, and PsbR polypeptides (Agrisera codes AS05092, AS06167, AS06142-16, and AS05059, respectively), using the alkaline phosphatase conjugate method, with 5-bromo-4-chloro-3-indolyl phosphate/nitro blue tetrazolium as chromogenic substrates (Sigma-Aldrich).

Mass spectrometry and chromatographic conditions

For liquid chromatography tandem mass spectrometry (LC–MS/MS) analysis, spots from the 2D SDS-PAGE were cut out and proteins digested in-gel with trypsin (code V5111, Promega), as described in Hellmann et al. (1995).

LC–MS/MS analyses were performed by a micro-LC Eksigent Technologies (Dublin, USA) system that included a micro LC200 Eksigent pump with flow module 5-50 µL and a programmable autosampler CTC PAL with a Peltier unit (1.0–45.0 °C). The stationary phase was a Halo Fused C18 column (0.5 × 100 mm, 2.7 µm; Eksigent Technologies Dublin, USA). The mobile phase was a mixture of 0.1 % (v/v) formic acid in water (A) and 0.1 % (v/v) formic acid in acetonitrile (B), eluting at a flow-rate of 15.0 mL min^{-1} and at an increasing concentration of solvent B from 2 to 40 % in 30 min. The injection volume was 4.0 µL. The oven temperature was set at 40 °C.

The LC system was interfaced with a 5600^{+} Triple-TOF^{TM} system (AB SCIEX, Concord, Canada) equipped with DuoSprayTM Ion Source and CDS (Calibrant Delivery System). The mass spectrometer worked in information-dependent acquisition (IDA) mode. Peptide profiling was performed using a mass range of 100–1600 Da (TOF scan with an accumulation time of 100.0 ms), followed by a MS/MS product ion scan from 200 to 1250 Da (accumulation time of 5.0 ms) with the abundance threshold set at 30 cps (35 candidate ions can be monitored per cycle). The ion source parameters in electrospray positive mode were set as follows: curtain gas (N_2) at 25 psig, nebulizer gas GAS1 at 25 psig, and GAS2 at 20 psig, ionspray floating voltage (ISFV) at 5000 V, source temperature at 450 °C and declustering potential at 25 V.

MS data were acquired with Analyst TF 1.7 (AB SCIEX, Concord, Canada). Subsequently, PeakView version 2.1 (AB SCIEX, Concord, Canada) was used to generate Mascot (.mgf) files with peak lists from the Analyst software files (.wiff); the default parameters were used (http://www.matrixscience.com).

The MS/MS spectra obtained by digested samples were analyzed as Mascot generic files against all entries in the public NCBInr database using the online Mascot server (Matrix Science: http://www.matrixscience.com/) without a taxonomy filter.

The principal parameter settings for the Mascot search were as follows: database NCBInr (version 2015.04.25; containing 65,519,838 sequence entries); enzyme trypsin; allow up to one missed cleavage; possible variable modifications carbamidomethylation of cysteine (C), oxidation of methionine (M), deamidation of asparagine and glutamine (NQ); precursor ion mass and fragment masses tolerance of 60 ppm and 0.3 Da, respectively; instrument default; default charge state set to 2+, 3+, and 4+. Widely accepted positive identifications of proteins by MS/MS analysis require a minimum of two unique peptides with at least one peptide having a significant ion score ($p \leq 0.05$). Considering that the genome of *Pisum sativum* is not fully sequenced, and that only some protein sequences of *P. sativum* are present in the database, we also accepted hits identified by at least one peptide with a significant ion score according to the MASCOT MS/MS ion search algorithm as being confident assignments.

Transmission electron microscopy and single-particle image analysis

PSII-LHCII megacomplexes from the analyzed sucrose gradient band, immediately after isolation, were applied to glow discharged carbon-coated copper grids, washed with distilled water, and negatively stained with 2 % (w/v) uranyl acetate. After checking the reproducibility of the preparation by preliminary TEM analyses on five independent-isolated samples, two datasets of images were collected from two individual samples chosen as

representative of the preparation, and then subsequently merged. For acquisition of micrographs, a FEI Tecnai F20-ST transmission electron microscope, equipped with a field emission gun (FEG) operated at 200 keV, was used. A total of 339 images were recorded at 29,000× on a Gatan Orius 4.0 K x 2.7 K CCD camera, leading to a final pixel size of 3.4 Å at the specimen level. Imaging conditions were optimized, in terms of defocus and astigmatism, to ensure the first minima of the Fourier power spectrum was within 15 Å and an underfocus range of 0.5–1.5 μm present. Particles were floated out into boxes using the boxer module of EMAN2 (Tang et al. 2007). All latter image processing steps were performed within the IMAGIC-V software environment (Imagic Science GmbH, Berlin, Germany) (van Heel et al. 1996), including initial reference-free alignment, multi-reference alignments, multivariate statistical analyses and classification, Fourier ring correlation estimation, and as further described in van Heel et al. (2000). Relevant crystallographic co-ordinate atom and chain data (PDB IDs: 3ARC, 2BHW, 3PL9) were overlaid onto characteristic views derived from the single-particle sub-populations identified, using UCSF Chimera (Pettersen et al. 2004) modeling software.

Results and discussion

Isolation of PSII-LHCII megacomplexes

In previous work (Pagliano et al. 2012), conditions for the direct solubilisation of stacked thylakoid membranes isolated from pea leaves were optimized in order to solubilize high molecular mass PSII-LHCII complexes. In so doing, it was found that after treating isolated-stacked pea thylakoids, at a Chl concentration of 1 mg mL^{-1}, with α-DDM concentrations ranging between 50 and 100 mM for 1 min, an almost complete solubilization of the entire membrane compartments could be achieved and well-defined high molecular mass PSII-LHCII complexes solubilized with high reproducibility (Pagliano et al. 2012). The amount and molecular mass of solubilized PSII-LHCII complexes did not change even when longer times of solubilization (10 and 30 min) were tested (data not shown), attesting that the duration of the solubilization, at least in these experimental conditions, does not lead to either aggregation or dissociation of PSII-LHCII complexes. By solubilizing stacked pea thylakoid membranes at a Chl concentration of 1 mg mL^{-1}, for the shortest time tested (1 min) and with the lowest concentration of α-DDM (50 mM) effective in solubilizing high molecular mass PSII-LHCII complexes, followed by a relatively quick (12 h) ultracentrifugation step on a sucrose density gradient, we isolated homogenous preparations of PSII-LHCII

supercomplexes, subsequently used for structural studies (Barera et al. 2012; Pagliano et al. 2014). In detail, in the gradient five different green bands, termed α1 to α5, were separated: band α1 contained mostly LHCII trimers; band α2 was composed of PSI-LHCI complexes co-migrating with ATP-ase; and bands α3 to α5 were observed to be composed predominantly of PSII-LCHII particles (Fig. 1). Band α3 has been characterized previously (Barera et al. 2012) and corresponds to PSII-LHCII supercomplexes of type $C_2S_2M_2$. This latter preparation was also used as starting material for single-particle electron microscopy studies that led to a three-dimensional model of the supercomplex of type $C_2S_2M_2$ from pea plants (Pagliano et al. 2014). The lower, highly reproducible bands of the gradient, α4 and α5, given their higher apparent molecular mass, were expected to contain either PSII-LHCII supercomplexes of increasing size, or even larger forms of PSII-LHCII, termed megacomplexes. In the work presented here, therefore, a detailed biochemical and structural characterization of band α5 was performed, this being the heaviest and most abundant of the two bands observed.

Spectroscopic characterization of PSII-LHCII megacomplexes

The absorption spectrum of band α5 is presented in Fig. 2a. The α5 particles registered absorption peaks at 436, 469, and 677 nm, similar to values previously observed for PSII-LHCII supercomplexes of type $C_2S_2M_2$ present in band α3 of the sucrose gradient (see Barera et al. 2012). The relatively high intensity of the absorption in the Chl b region (470 and 650 nm) of band α5, together with its
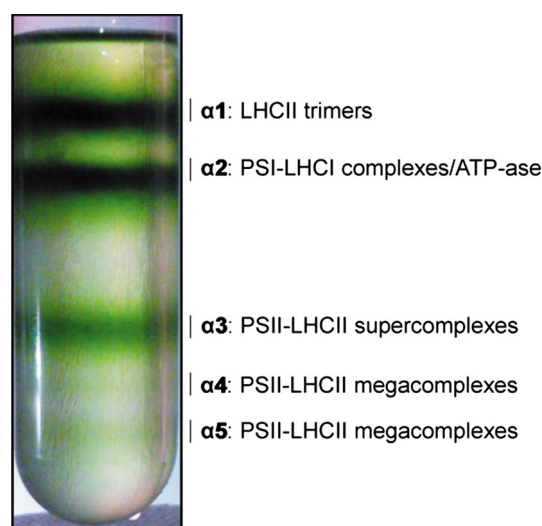

Fig. 1 Isolation of PSII-LHCII megacomplexes by sucrose density gradient ultracentrifugation of pea thylakoid membranes solubilized with α-DDM
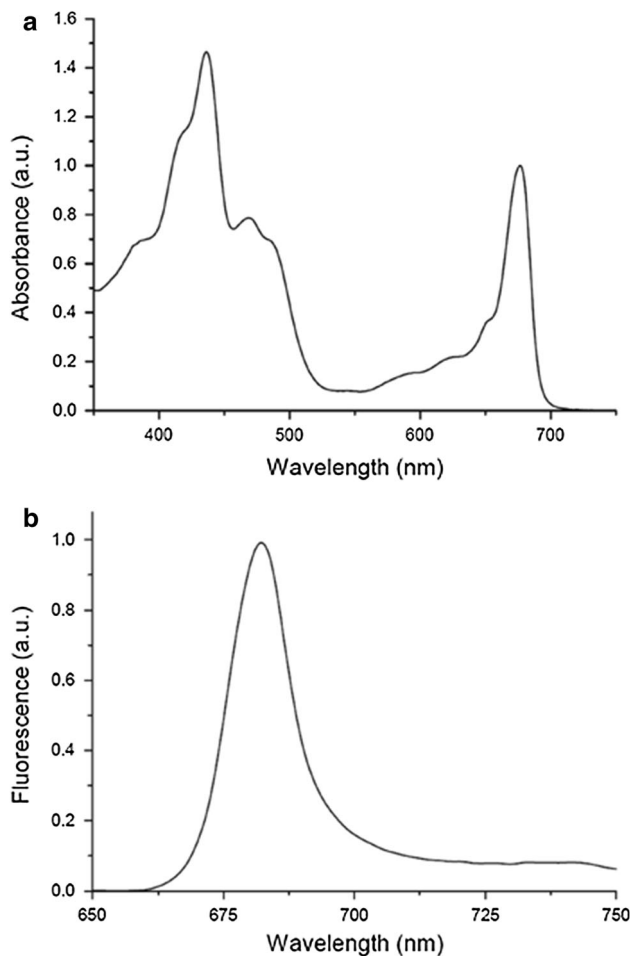
Fig. 2 Absorption spectrum normalized to the maximum in the *red region* (**a**) and low-temperature (77 K) fluorescence emission spectrum normalized to the maximum value (**b**) obtained from sucrose gradient band α5

Chl *a/b* ratio between 2.4 and 2.6, is consistent with studies conducted on forms of PSII isolated directly from thylakoid membranes that are larger than the basic C_2S_2 unit and enriched in the Lhcb6 antenna subunit (Eshaghi et al. 1999; Barera et al. 2012). It should be noted that the 2.4–2.6 ratio is lower than values typically observed for PSII-LHCII supercomplexes of type C_2S_2 (Eshaghi et al. 1999; Barera et al. 2012).

The low-temperature emission spectrum of the α5 particles is shown in Fig. 2b. It reveals a single-fluorescence emission peak at 683 nm, an intermediate value compared to that of PSII-LHCII supercomplexes of type C_2S_2 (682 nm) and $C_2S_2M_2$ (684 nm) (see Barera et al. 2012). Performing fluorescence studies at 77 K can give valuable information on the structural organization of the photosynthetic apparatus (van Grondelle et al. 1994). Detailed 77 K fluorescence studies have shown that PSII has two main emission bands at 685 and 695 nm, corresponding to two different Chl-protein complexes of PSII: the RC and

core antenna complexes, respectively (Dekker et al. 1995). An additional peak at 680 nm has been ascribed to the LHCII originating from the red-most Chl *a* pigment in LHCII, absorbing at 676 nm (Hemelrijk et al. 1992). For the PSII-LHCII particles of band α5 (see Fig. 2b), the main peak at 683 nm is red-shifted compared to the expected characteristics of the LHCII trimers alone, confirming that there is energy transfer between LHCII and the PSII core complex. Notably, there is no 77 K fluorescence peak at 735 nm, confirming the absence of any PSI contamination in the α5 particles (Gobets and van Grondelle 2001).

Protein composition of PSII-LHCII megacomplexes

In order to investigate the oligomerization state of the isolated high molecular mass PSII-LHCII containing particles present in band α5, and search for any counterpart within the original thylakoid membranes, large-pore blue native PAGE (lpBN-PAGE) was performed either on isolated particles or on thylakoids. In Fig. 3a, the lpBN-PAGE profile of the band α5 is shown and compared to that of thylakoid membranes solubilized with α-DDM under the same conditions used for band α5 isolation. In these lpBN-PAGE profiles, the high molecular mass region showed: (1) a variable number of bands with molecular masses falling within the region 669–2000 kDa, with three such bands detectable only after Coomassie staining in the band α5 and, intriguingly, four such bands being predominant in solubilized thylakoids; (2) three green bands with molecular masses above 2000 kDa, predominant in the α5 sample, and also detectable in solubilized thylakoids. The nature of these high molecular mass PSII-LHCII containing complexes was probed by performing the denaturing 2D SDS-PAGE of the native PAGE lanes of the thylakoid membranes and of band α5, whose profiles, after silver staining, are shown in Fig. 3b and supplementary Fig. S1a, respectively. In Fig. 3c, an enlargement of the region above 2000 kDa of the denaturing 2D SDS-PAGE of the band α5 of Fig. S1a is shown. The denatured second-dimension profile of the lpBN-PAGE of solubilized thylakoids, interpreted according to previous reports (Aro et al. 2005; Granvogl et al. 2006; Pagliano et al. 2012, 2014), revealed that: (1) the four bands with molecular masses between 669 and 2000 kDa were indeed PSII-LHCII supercomplexes of different sizes, one with a lower mass containing only LHCII S-trimers; the further three, with increasing molecular masses, containing additional LHCII M-trimers; (2) the bands with molecular masses above 2000 kDa contained PSII-LHCII megacomplexes, given a protein composition similar to that displayed by PSII-LHCII supercomplexes, but a molecular mass over twice that of the supercomplex with smaller size. Hence, by comparing the denaturing second-dimension profile of the lpBN-
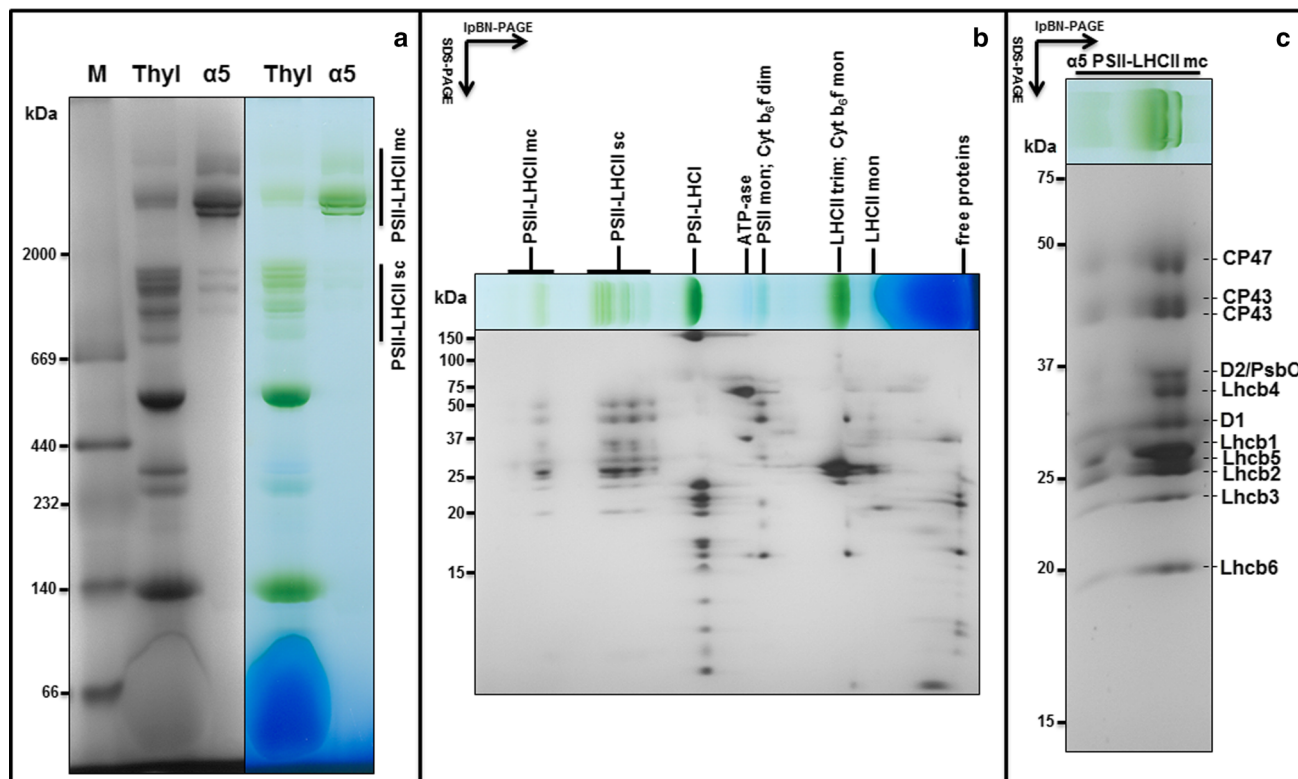
Fig. 3 Electrophoretic separation of pea thylakoid membranes solubilized with α-DDM and sucrose gradient band α5. **a** lpBN-PAGE of solubilized thylakoids (25 µg Chl) and of band α5 (6 µg Chl), Coomassie stained and non Coomassie stained. *Lane M* mixture of native high molecular weight marker (GE Healthcare) and blue dextran (Sigma-Aldrich). **b, c** Silver-stained second-dimension SDS-PAGEs of solubilized thylakoids and of the PSII-LHCII mc region of band α5, respectively. Labels on the *left* indicate the molecular weight marker positions (Bio-Rad precision plus). In **b** identification of the macromolecular protein complexes of thylakoid membranes is given on the *top* of the gel. Isolated complexes were indexed as follows: megacomplex (mc), supercomplex (sc), trimer (trim), dimer (dim), monomer (mon). In **c** identification of the polypeptide composition of the PSII-LHCII mc region of band α5 by MS/MS spectrometry (see also Table S1)

PAGE of band α5 (Figs. S1a, 3c) to that of the solubilized thylakoid membranes (Fig. 3b), it was clear the analogous nature of PSII-LHCII supercomplexes for the faint bands lying between 669 and 2000 kDa and that of PSII-LHCII megacomplexes for the predominant bands, in the region >2000 kDa (hereafter referred to as α5 PSII-LHCII mc region). The low amount of PSII-LHCII supercomplexes with respect to the predominant content of PSII-LHCII megacomplexes found in band α5 might be taken as an indication of the relatively high molecular stability of the isolated PSII-LHCII megacomplexes. Moreover, the detection of their counterparts within the solubilized thylakoid membranes would suggest that the isolation step by sucrose gradient ultracentrifugation maintains the genuine nature of megacomplexes of these high molecular mass PSII-LHCII complexes.

After in-gel trypsin digestion of all the spots stained on the second dimension of the α5 PSII-LHCII mc region, micro-LC-ESI–MS/MS analysis of the digested peptides revealed the presence of the RC core subunits D2 and D1, the inner antenna proteins CP47 and CP43, the six Lhcb outer antenna proteins (Lhcb1-6), and the OEC subunit PsbO (see supplementary Table S1), thus allowing their positions on the 2D SDS-PAGE map to be identified (Fig. 3c). The detection of the Lhcb3 and Lhb6 antennae subunits, the former being an exclusive component of LHCII M-trimers (Boekema et al. 1999a), and the latter a linker for the LHCII M-trimer to the C_2S_2 supercomplex (Barera et al. 2012) confirmed the occurrence of LHCII M-trimers in the preparation. In particular, the proteomic analysis proved the existence of at least three distinguishable sub-populations of PSII-LHCII megacomplexes in the preparation, visible in the α5 PSII-LHCII mc region (Fig. 3c), with different sizes and containing LHCII M-trimers.

For the particles of band α5, Western blot analyses for the OEC polypeptides, based on identical Chl loading (Fig. 4), showed the presence of a high quantity of PsbO, a low amount of PsbP, and the absence of PsbQ and PsbR. In band α5 the presence of the subunit PsbO bound to the PSII-LHCII megacomplexes particles was confirmed by MS/MS analysis (see Table S1; Fig. 3c), and that of PsbP
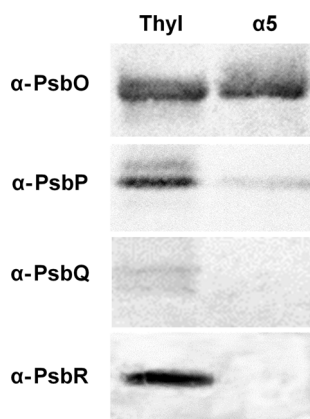
Thyl   α5

α-PsbO

α-PsbP

α-PsbQ

α-PsbR

Fig. 4 Western blot with antibodies against the extrinsic subunits PsbO, PsbP, PsbQ, and PsbR of sucrose gradient band α5 and of thylakoid membranes. The same amount of Chl (4 μg) was loaded on each lane

by Western blot analysis performed on the second dimension of the entire lpBN-PAGE lane of band α5 (Fig. S1b, see the low amount in the PSII-LHCII mc region between 20 and 25 kDa).

Determination of the supramolecular structure of PSII-LHCII megacomplexes

PSII-LHCII megacomplexes, immediately after isolation from band α5 by sucrose density gradient ultracentrifugation, were adsorbed onto carbon film, washed with distilled water, and negatively stained using uranyl acetate. The reproducibility of the preparation was checked by preliminary TEM imaging upon five independent-isolated samples. In Fig. 5a micrograph, chosen as representative of the preparation, shows the distribution on the carbon support of
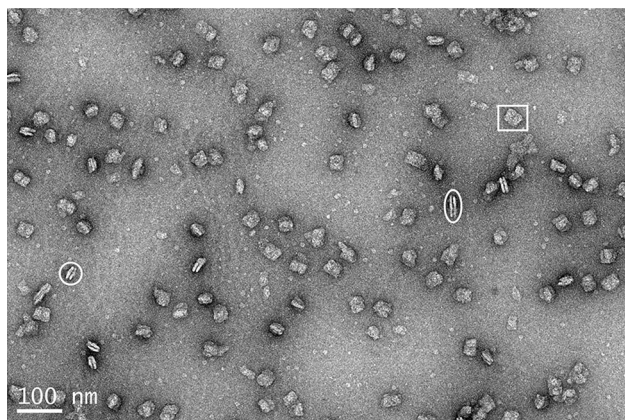

Fig. 5 Electron micrograph of sucrose gradient band α5 particles, negatively stained with 2 % uranyl acetate. *Top-view*, *side-view* and *end-view* projections of the megacomplexes are indicated by *white rectangles*, *ovals* and *circles*, respectively. The *scale bar* represents 100 nm

the particles present in band α5. PSII-LHCII megacomplexes in top-, side-, and end-view orientations are clearly discernible; in addition, many large particles are present in tilted view, most likely PSII-LHCII megacomplexes, with a low amount of C_2S_2 PSII-LHCII supercomplexes in top-view orientation and some small particles, possibly detached LHCIIs.

To compile the single-particle image dataset, TEM images from two independent samples were recorded at a sampling frequency of 3.4 Å per pixel using a consistent ~ 1 μm underfocus, equating to the first minimum of the contrast transfer function being ~ 15 Å, and then merged. All possible single particles, i.e., intact or degraded, were selected, resulting in a total of 8963 available 2D projections of varying orientation. The dataset was processed by reference-free alignment and multivariate statistical analysis. Over five iterations of refinement, ~ 5 % of particles were set inactive at each stage to ameliorate against the heterogeneous nature of the raw data, resulting in 1792 particles being excluded and 600 class averages being requested from 7171 particles (see supplementary Fig. S2). The averages displayed a greatly improved signal-to-noise ratio over the raw dataset of particle images and subjectively represented the most relevant spread of variation for observing characteristic views.

About one third of the entire dataset consisted of particles ascribed to top-, side-, and end-view orientations, the rest being considered tilted views of intermediate orientation (see Table 1). Among the particles seen in top view, ~ 14 % were attributed to single, non-sandwich, PSII-LHCII supercomplexes of type C_2S_2, C_2S_2M, and $C_2S_2M_2$ (Table 1). No single supercomplexes were observed in side-view orientation, but the possibility does remain that further non-sandwich supercomplex projections may exist within the averages of other tilted orientations observed in the total classification (see Fig. S2). However, such a minute percentage is in agreement with the low quantity of PSII-LHCII supercomplexes revealed in band α5 by electrophoretic methods (see Figs. 3a, S1a). Roughly 86 % of the particles seen in top, side, and end view were ascribable to PSII-LHCII megacomplexes (see Table 1), these resulting the predominant complexes within band α5. This would suggest that a strong supramolecular interaction exists between PSII-LHCII supercomplexes when they constitute larger complexes. Among these, the most intact and striking views were attributed to top, side and end views of the PSII-LHCII megacomplexes shown in Fig. 6a, specifically those classes numbered 1 and 4 for top views, class 2 for a side view, and class 3 for an end view. All averages shown are ~ 18 Å in resolution as estimated by Fourier ring correlation. The number of raw particles for these classes is shown in Table 1 and their domain arrangement is proposed with labels in white on Fig. 6a

Table 1 Relative occurrence of the various PSII-LHCII supercomplexes and megacomplexes in the sucrose gradient band α5 of Fig. 1. Values are based on two datasets (see text) of 8963 particles collected in total from two independently isolated bands α5

	Number of particles observed	% total particles analyzed
Initial dataset of picked particles	8963	–
Junk particles removed by processing	1792	–
Total image-processed dataset (see Fig. S2)	7171	100
Tilted views of intermediate orientation	4987	69.5
Top/side/end views	2184	30.5

Complex—nomenclature according to Dekker and Boekema (2005), [Schönflies notation point group symmetry]	Number of particles observed	% total top/side/end views
Supercomplex C_2S_2 top views [C2, single PSII dimeric core] (see Fig. S2)	35	1.6
Supercomplex C_2S_2M top views [C2, single PSII dimeric core] (see Fig. S2)	167	7.7
Supercomplex $C_2S_2M_2$ top views [C2, single PSII dimeric core] (see Fig. S2)	99	4.5
Total supercomplexes	301	13.8
Megacomplex $(C_2S_2)_4$ top views [intact D2, four copies of PSII dimeric core] (see Fig. 6, location 1)	403	18.5
Megacomplex $(C_2S_2)_4$ end views [intact D2, four copies of PSII dimeric core] (see Fig. 6, location 3)	38	1.7
Megacomplex $(C_2S_2)_{2 \text{ or } 4}$ side views [intact D2, four copies of PSII dimeric core] (see Fig. 6, location 2)	878	40.2
Megacomplex $(C_2S_2 + C_2S_2M_2)_2$ top views [intact D2, four copies of PSII dimeric core] (see Fig. 6, location 4)	320	14.7
Megacomplex $C_2S + (C_2S_2)_2$ top views [broken symmetry, three copies of PSII dimeric core] (see Fig. S2)	244	11.1
Total megacomplexes	1883	86.2
Total supercomplexes + megacomplexes	2184	100

(according to Dekker and Boekema 2005), where C represents a PSII core monomer, S the strongly bound LHCII trimer and M the moderately bound LHCII trimer. No obvious views were observed that would suggest the presence of LHCII L-trimers loosely bound to the PSII core.

A novel arrangement of four C_2S_2 supercomplexes was observed, where two were bound side-by-side in the plane of the membrane and then further sandwiched together with a second copy; these high molecular mass complexes, with an estimated molecular mass of at least 4.4 MDa, were termed $(C_2S_2)_4$ megacomplexes. Such a macromolecular form was immediately obvious in both top and end view orientations (locations 1 and 3, Fig. 6a), in total representing 23.4 % of the 1883 particles, unequivocally attributable to megacomplexes present in the dataset (see Table 1). The percentage of this form of megacomplex may increase to ∼70 % if the side views of location 2 are considered exclusively as $(C_2S_2)_4$ sandwich particles, but the presence of $(C_2S_2)_2$ sandwich particles within these

side-view averages may not be excluded, since these would not be discernible in this orientation. The overall top view dimensions of the megacomplex were, at most, 410 Å in width (x) and 350 Å in length (y), with an internal corner-to-corner diagonal of 450 Å. Any height (z) of the side views must be inclusive of the lumenally bound PSII subunits known to optimize the water-splitting environment, identified in this study as PsbO and PsbP (see Figs. 3c, 4, S1b; Table S1). These lumenal protrusions are clearly present, extending out from the membrane domain of the side view and end view of locations 2 and 3 (Fig. 6a). The height (z) of the side view sandwich is 290 Å and, within it, each single side view, therein, being 145 Å (z), of which 60–65 Å may be attributed to the extrinsic lumenally protruding subunits. Taken as a whole, these views of the new megacomplex form show that it is a sandwich, the top half viewed from the lumenal surface sitting on top of an identical copy, viewed from underneath. The result is that the internal "diagonal" appearance of the single-dimeric PSII core, typically being top left to
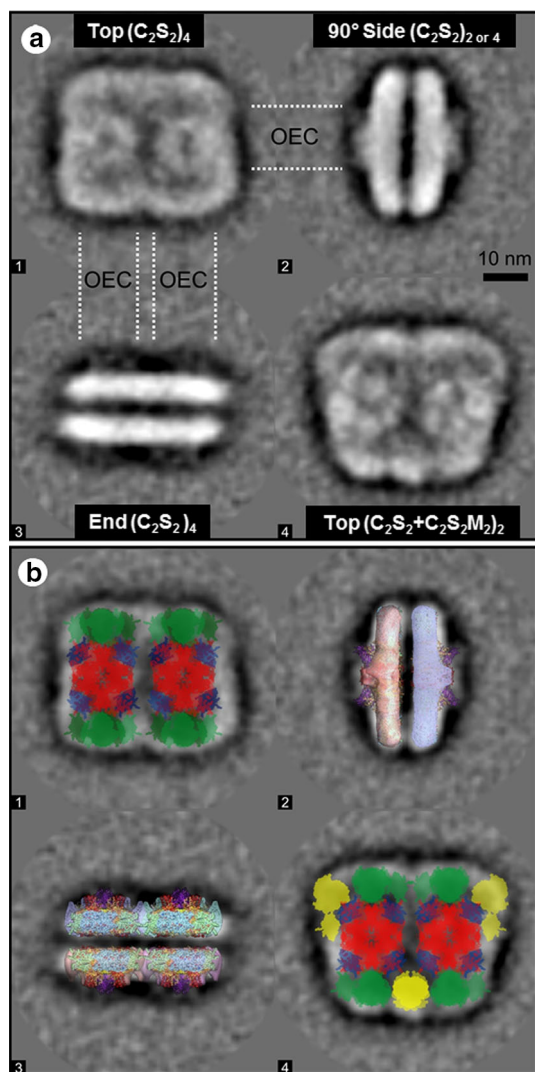
maps presented in Pagliano et al. (2014), due to the relative lack of tilted views present within the negatively stained data used; however, one could speculate that this second protruding lumenal domain might be a candidate for the position of PsbP, in accordance also with a similar positioning of this subunit within the PSII-LHCII supercomplex by Ido et al. (2014). The use of Protein Databank (.pdb) files for modeling purposes with the program UCSF Chimera was extended to include all-atom spheres for each PSII and LHCII subunit, assigned as in Pagliano et al. (2014) (Fig. 6b). The presence of sandwiched particles necessarily increases the complexity of any attempted domain assignment process for further novel characteristic views classified, but such an exercise aids in understanding the majority of views observed. The other most prevalent class of top view intact particles is shown in location 4 (Fig. 6a), representing 17 % of the 1883 particles univocally attributable to megacomplexes present in the dataset (see Table 1). From many models attempted (data not shown), it was concluded that location 4 represents a top view of a sandwiched megacomplex that must include two moderately bound LHCII M-trimers within each half of the megacomplex sandwich, in addition to two C_2S_2 units, thus forming a $(C_2S_2 + C_2S_2M_2)_2$ megacomplex. Sandwich-form megacomplexes in three dimensions, once projected down into two-dimensional views, will result in a complex overlapping arrangement of atoms. An expanded interpretation of the sandwich-form megacomplexes of locations 1 and 4 is offered in Fig. 6b, the former shown as a lumenally viewed ($C_2S_2 + C_2S_2$) megacomplex merged atop a

bottom right when observed in top view (see Barera et al. 2012), is obscured to form a square, multi-domain arrangement when viewed in 2D projection from the lumenal surface of a sandwich megacomplex (locations 1 and 4). To aid the reader further, four copies of the 3D map of a C_2S_2 supercomplex, reported previously (Pagliano et al. 2014), were imported into a UCSF Chimera modeling environment (Fig. 6b) and overlaid onto locations 2 and 3. The color of these maps was chosen arbitrarily, but the two side-by-side C_2S_2 supercomplex 3D maps of the top half of the sandwich are colored purple and cyan using a see-through mesh render, whereas the other half of the megacomplex sandwich, two side-by-side C_2S_2 supercomplex 3D maps viewed from underneath, are orange and magenta solid surface representations. In addition to the central lumenally protruding domain, attributable to the PsbO subunit, the 3D maps (Fig. 6b) contain a second protruding lumenal domain off the edge of each PSII monomer. Caution was urged regarding the interpretation of the 3D

stromally viewed (C_2S_2 + C_2S_2) megacomplex, and the latter as a lumenally viewed (C_2S_2 + $C_2S_2M_2$) megacomplex merged atop a stromally viewed ($C_2S_2M_2$ + C_2S_2) megacomplex. The 3D maps and schematic representations used in Fig. 6b aid in visualizing the interactions between the stromal surfaces of PSII-LHCII supercomplexes in the two halves of the sandwich, forming the stromal gap. Contacts between PSII and LHCII supercomplexes in adjacent membranes are mediated by the stromal flat surfaces of both the LHCs and the PSII reaction center dimers. The LHCII trimers at either end of one supercomplex sit atop the LHCII trimers of the supercomplex in the opposite membrane. The interaction of LHCII trimers with one another in grana thylakoids, like molecular Velcro, is supported either by the charge complementarity shown in the atomic structure of the trimeric LHCII proposed by Standfuss et al. (2005) or by the direct tomographic observations in pea chloroplast membranes (Daum et al. 2010). The overall geometry of the interaction between the stromal surfaces of the PSII-LHCII supercomplexes in two adjacent membranes is similar to that observed in isolated supercomplex sandwich dimers by single-particle cryo-TEM (Nield et al. 2000), although different for a rotational offset of ~90° from that displayed by PSII-LHCII supercomplexes that form ordered 2D arrays in the grana observed by tomography (Daum et al. 2010). It can not be excluded that the similarity with other isolated supercomplex sandwiches is related to the unavoidable use of detergents during the purification step. Nevertheless, two different detergents, α-DDM (in this study) and β-DDM (Nield et al. 2000), have been used for comparable structural studies (Nield et al. 2000; Barera et al. 2012; Pagliano et al. 2014), the former considered milder and more effective than the latter in solubilizing larger PSII-LHCII complexes from stacked thylakoid membranes (see Pagliano et al. 2012). The isolated megacomplexes of this study derive from a complete solubilization of the thylakoid membranes of pea plants grown at moderate light (i.e., 150 μmol m^{-2} s^{-1} photons). Therefore, they can likely be considered possible representatives of the supramolecular arrangements of PSII-LHCII supercomplexes within thylakoids of plants acclimated to this light condition, and not exclusively within local patches of semicrystalline 2D arrays that occur occasionally in grana membranes, at higher frequency in low-light-treated plants (Daum et al. 2010; Kouřil et al. 2013). This observation, together with the fact that the isolated megacomplexes displayed additional antenna proteins (i.e., LHCII M-trimers present at least in one class of isolated megacomplexes, see Fig. 6 location 4) bound to the basic C_2S_2 units, might explain the different geometry present at the conjoint stromal surfaces for PSII-LHCII supercomplexes in two adjacent membranes, differently to that observed in

tomograms of 2D arrays of C_2S_2 PSII-LHCII supercomplexes by Daum et al. (2010).

During the preparation of the TEM grid, the detachment of some LHCIIs (i.e., monomeric LHCIIs, and trimeric LHCIIs of type M and even S) from the band α5 megacomplexes may not be excluded, since an amount of small particulate matter remains visible in the background of the TEM images (see Fig. 5) and the occurrence of megacomplexes with broken symmetry, likely of type C_2S + (C_2S_2)$_2$, was observed during the classification (see Table 1; Fig. S2). The detachment of some LHCIIs from the megacomplexes might be partially induced by the experimental technique of washing the samples on the grid with water, prior to the negative-stain fixation. This technique is well known to improve the imaging by lowering the stain background, through the dilution of the high sucrose concentration present within sucrose gradients bands (>1 M in the isolated band α5). Notwithstanding the low amount of detached LHCIIs and supercomplexes observed, the majority of the particles in this preparation were stable PSII-LHCII megacomplexes, in a sandwich form, characterized by two new types of symmetrical organization.

Concluding remarks

A direct method for the isolation of pure PSII-LHCII megacomplexes has been demonstrated, consisting of a single-rapid (1 min) solubilization of stacked pea thylakoid membranes with α-DDM at experimental conditions that effectively solubilize entire thylakoids, followed by a relatively quick (12 h) ultracentrifugation step using continuous sucrose density gradients. Spectroscopic and proteomic analyses revealed that the heaviest band of the sucrose gradient contained pure PSII-LHCII megacomplexes. TEM analyses on negatively stained samples, and classification of the single-particle views observed therein, revealed the presence of megacomplexes having a novel structure compared to that reported previously (Boekema et al. 1999a, b), whereby two PSII-LHCII supercomplexes sit side-by-side in the membrane plane, interacting with a second-inverted copy of a similar megacomplex forming a sandwich organization. Two predominant forms of intact sandwiched megacomplexes were observed, a (C_2S_2)$_4$ megacomplex and a (C_2S_2 + $C_2S_2M_2$)$_2$ megacomplex. The (C_2S_2)$_4$ megacomplex displayed a central arrangement of two C_2S_2 supercomplexes, interacting with an intra-membrane plane twofold symmetry; the organization of the second copy of two C_2S_2 supercomplexes in the other appressed membrane is related to the first layer by a 180° rotation about an axis at a position half way between the two membranes. The (C_2S_2 + $C_2S_2M_2$)$_2$ megacomplex differs from the (C_2S_2)$_4$

megacomplex by having two additional moderately bound LHCII M-trimers present within each half of the megacomplex sandwich, one peripheral and the other in a central position, making a bridge between the two supercomplexes in the same membrane plane. The occurrence of LHCII M-trimers in this preparation was further confirmed by proteomic analyses.

For a full understanding of plant photosynthesis, it is necessary to establish how the PSII-LHCII supercomplexes are organized and interact with one another in the highly dynamic thylakoid membranes. These new structural forms of isolated megacomplexes, and the modeling proposed, provide intriguing insights into how PSII-LHCII supercomplexes may bind to each other, in register, both in the membrane plane and between granal stacks within the chloroplast. We have provided evidence of different geometries for the interaction between the stromal surfaces of PSII-LHCII supercomplexes across two adjacent membranes, in addition to those proposed by Daum et al. (2010) for the case of thylakoid patches containing crystalline 2D arrays of C_2S_2 supercomplexes. Noteworthy, however, is the fact that, despite the different starting material, either plant (i.e., spinach or pea) or preparation (i.e., native chloroplasts/thylakoids or isolated complexes; chloroplasts/thylakoids exposed to light or megacomplexes isolated in the dark during the purification step), the direct interaction between LHCII trimers of the supercomplexes in the two adjacent membranes is maintained. Therefore, it seems reasonable to conclude that the transmembrane interactions, holding two PSII-LHCII half-sandwiches together in the isolated megacomplexes, are very similar to those that govern granal stacking in PSII-LHCII 2D arrays in native chloroplasts and that the electrostatic interactions between LHCII trimers are a key factor in this stacking.

In summary, the overall data collected on these isolated sandwiched megacomplexes will improve our understanding of the arrangement of PSII and its LHCII antenna system in chloroplast membranes of higher plants, complementing the structural work performed by cryo-electron tomography on native thylakoid membranes and the sectioning of intact chloroplasts (Daum et al. 2010).

References

Albertsson PA (2001) A quantitative model of the domain structure of the photosynthetic membrane. Trends Plant Sci 6:349–354

Amunts A, Nelson N (2009) Plant photosystem I design in the light of evolution. Structure 17:37–650

Andersson B, Anderson JM (1980) Lateral heterogeneity in the distribution of chlorophyll-protein complexes of the thylakoid membranes of spinach. Biochim Biophys Acta 593:427–440

Arnon DJ (1949) Copper enzymes in isolated chloroplasts, polyphenoloxidase in *Beta vulgaris*. Plant Physiol 24:1–14

Aro EM, Suorsa M, Rokka A, Allahverdiyeva Y, Paakkarinen V, Saleem A, Battchikova N, Rintamaki E (2005) Dynamics of photosystem II: a proteomic approach to thylakoid protein complexes. J Exp Bot 56:347–356

Balsera M, Arellano JB, Revuelta JL, De Las Rivas J, Hermoso JA (2005) The 1.49 Å resolution crystal structure of PsbQ from photosystem II of *Spinacia oleracea* reveals a PPII structure in the N-terminal region. J Mol Biol 350:1051–1060

Barber J (1982) Influence of surface charges on thylakoid structure and function. Annu Rev Plant Physiol 33:261–295

Barera S, Pagliano C, Pape T, Saracco G, Barber J (2012) Characterization of PSII-LHCII supercomplexes isolated from pea thylakoid membrane by one-step treatment with α- and β-dodecyl-D-maltoside. Philos Trans R Soc Lond B Biol Sci 367:3389–3399

Boekema EJ, van Roon H, Calkoen F, Bassi R, Dekker JP (1999a) Multiple types of association of photosystem II and its light-harvesting antenna in partially solubilized photosystem II membranes. Biochemistry 38:2233–2239

Boekema EJ, Van Roon H, Van Breemen JF, Dekker JP (1999b) Supramolecular organization of photosystem II and its light-harvesting antenna in partially solubilized photosystem II membranes. Eur J Biochem 266:444–452

Caffarri S, Croce R, Cattivelli L, Bassi R (2004) A look within LHCII: differential analysis of the Lhcb1-3 complexes building the major trimeric antenna complex of higher-plant photosynthesis. Biochemistry 43:9467–9476

Caffarri S, Kouřil R, Kereïche S, Boekema EJ, Croce R (2009) Functional architecture of higher plant photosystem II supercomplexes. EMBO J 28:3052–3063

Calderone V, Trabucco M, Vujičić A, Battistutta R, Giacometti GM, Andreucci F, Barbato R, Zanotti G (2003) Crystal structure of the PsbQ protein of photosystem II from higher plants. EMBO Rep 4:900–905

Daum B, Nicastro D, Austin JIII, McIntosh R, Kühlbrandt W (2010) Arrangement of photosystem II and ATP synthase in chloroplast membranes of spinach and pea. Plant Cell 22:1299–1312

Dekker JP, Boekema EJ (2005) Supramolecular organization of thylakoid membrane proteins in green plants. Biochim Biophys Acta 1706:12–39

Dekker JP, Hassoldt A, Pettersson A, van Roon H, Groot ML, van Grondelle R (1995) On the nature of the F695 and F685 emission of photosystem II. In: Mathis P (ed) Photosynthesis: from light to biosphere. Kluwer Academic Publishers, Dordrecht, pp 53–56

Eshaghi S, Andersson B, Barber J (1999) Isolation of a highly active PSII-LHCII supercomplex from thylakoid membranes by a direct method. FEBS Lett 446:23–26

Gobets B, van Grondelle R (2001) Energy transfer and trapping in photosystem I. Biochim Biophys Acta 1507:80–99

Granvogl B, Reisinger V, Eichacker LA (2006) Mapping the proteome of thylakoid membranes by de novo sequencing of intermembrane peptide domains. Proteomics 6:3681–3695

Groth G, Pohl E (2001) The structure of the chloroplast F1-ATPase at 3.2 Å resolution. J Biol Chem 276:1345–1352

Hankamer B, Barber J, Boekema E (1997) Structure and membrane organization of photosystem II in green plants. Annu Rev Plant Physiol Plant Mol Biol 48:641–671

Hankamer B, Morris EP, Nield J, Gerle C, Barber J (2001) Three dimensional structure of the photosystem II core dimer of higher plants determined by electron microscopy. J Struct Biol 135:262–269

Hellmann U, Wernstedt C, Gonez J, Heldin CH (1995) Improvement of an "In-Gel" digestion procedure for the micropreparation of internal protein fragments for amino acid sequencing. Anal Biochem 224:451–455

Hemelrijk PW, Kwa SLS, van Grondelle R, Dekker JP (1992) Spectroscopic properties of LHCII, the main light-harvesting chlorophyll a/b protein complex from chloroplast membranes. Biochim Biophys Acta 1098:159–166

Ido K, Nield J, Fukao Y, Nishimura T, Sato F, Ifuku K (2014) Cross-linking evidence for multiple interactions of the PsbP and PsbQ proteins in a higher plant photosystem II supercomplex. J Biol Chem 289:20150–20157

Ifuku K, Nakatsu T, Kato H, Sato F (2004) Crystal structure of the PsbP protein of photosystem II from Nicotiana tabacum. EMBO Rep 5:362–367

Jackowski G, Kacprzak K, Jansson S (2001) Identification of Lhcb1/Lhcb2/Lhcb3 heterotrimers of the main light-harvesting chlorophyll a/b-protein complex of photosystem II (LHCII). Biochim Biophys Acta 1504:340–345

Jansson S (1994) The light-harvesting chlorophyll a/b binding proteins. Biochim Biophys Acta 1184:1–19

Järvi S, Suorsa M, Paakkarinen V, Aro EM (2011) Optimized native gel systems for separation of thylakoid protein complexes: novel super- and mega-complexes. Biochem J 439:207–214

Kirchhoff H, Hall C, Wood M, Herbstová M, Tsabari O, Nevo R, Charuvi D, Shimoni E, Reich Z (2011) Dynamic control of protein diffusion within the granal thylakoid lumen. Proc Natl Acad Sci USA 108:20248–20253

Kouřil R, Wientjes E, Bultema JB, Croce R, Boekema EJ (2013) High-light vs. low-light: effect of light acclimation on photosystem II composition and organization in Arabidopsis thaliana. Biochim Biophys Acta 1827:411–419

Laemmli UK (1970) Cleavage of structural proteins during the assembly of the head of bacteriophage T4. Nature 227:680–685

Liu ZF, Yan HC, Wang KB, Kuang TY, Zhang JP, Gui LL, An XM, Chang WR (2004) Crystal structure of spinach major light-harvesting complex at 2.72 Å resolution. Nature 428:287–292

Mullet JE (1983) The amino acid sequence of the polypeptide segment which regulates membrane adhesion (grana stacking) in chloroplasts. J Biol Chem 258:9941–9948

Nanba O, Satoh K (1987) Isolation of a photosystem II reaction center consisting of D-1 and D-2 polypeptides and cytochrome b-559. Proc Natl Acad Sci USA 84:109–112

Nevo R, Chuartzman SG, Tsabari O, Reich Z (2009) Architecture and plasticity of thylakoid membrane networks. In: Wada H, Murata N (eds) Lipids in photosynthesis. Springer, Berlin, pp 295–328

Nield J, Barber J (2006) Refinement of the structural model for the photosystem II supercomplex of higher plants. Biochim Biophys Acta 1757:353–361

Nield J, Orlova EV, Morris EP, Gowen B, van Heel M, Barber J (2000) 3D map of the plant photosystem two supercomplex obtained by cryoelectron microscopy and single particle analysis. Nat Struct Biol 7:44–47

Pagliano C, Barera S, Chimirri F, Saracco G, Barber J (2012) Comparison of the α and β isomeric forms of the detergent n-dodecyl-D-maltoside for solubilizing photosynthetic complexes from pea thylakoid membranes. Biochim Biophys Acta 1817:1506–1515

Pagliano C, Saracco G, Barber J (2013) Structural, functional and auxiliary proteins of photosystem II. Photosynth Res 116:167–188

Pagliano C, Nield J, Marsano F, Pape T, Barera S, Saracco G, Barber J (2014) Proteomic characterization and three-dimensional electron microscopy study of PSII-LHCII supercomplexes from higher plants. Biochim Biophys Acta 1837:1454–1462

Pan X, Li M, Wan T, Wang L, Jia C, Hou Z, Zhao X, Zhang J, Chang W (2011) Structural insights into energy regulation of light-harvesting complex CP29 from spinach. Nat Struct Mol Biol 18:309–316

Pettersen EF, Goddard TD, Huang CC, Couch GS, Greenblatt DM, Meng EC, Ferrin TE (2004) UCSF Chimera—a visualization system for exploratory research and analysis. J Comput Chem 25:1605–1612

Rhee KH, Morris EP, Barber J, Kühlbrandt W (1998) Three-dimensional structure of the plant photosystem II reaction centre at 8 Å resolution. Nature 396:283–286

Shevchenko A, Wilm M, Vorm O, Mann M (1996) Mass spectrometric sequencing of proteins silver-stained polyacrylamide gels. Anal Chem 68:850–858

Standfuss J, van Scheltinga ACT, Lamborghini M, Kühlbrandt W (2005) Mechanisms of photoprotection and nonphotochemical quenching in pea light harvesting complex at 2.5 Å resolution. EMBO J 24:918–928

Tang G, Peng L, Baldwin PR, Mann DS, Jiang W, Rees I, Ludtke SJ (2007) EMAN2: an extensible image processing suite for electron microscopy. J Struct Biol 157:38–46

Umena Y, Kawakami K, Shen JR, Kamiya N (2011) Crystal structure of oxygen-evolving photosystem II at a resolution of 1.9 Å. Nature 473:55–60

van Grondelle R, Dekker JP, Gillbro T, Sundstrom V (1994) Energy transfer and trapping in photosynthesis. Biochim Biophys Acta 1187:1–65

van Heel M, Harauz G, Orlova EV, Schmidt R, Schatz M (1996) A new generation of the IMAGIC image processing system. J Struct Biol 116:17–24

van Heel M, Gowen B, Matadeen R, Orlova EV, Finn R, Pape T, Cohen D, Stark H, Schmidt R, Schatz M, Patwardhan A (2000) Single-particle electron cryo-microscopy: towards atomic resolution. Q Rev Biophys 33:307–369

Yakushevska AE, Jensen PE, Keegstra W, van Roon H, Scheller HV, Boekema EJ, Dekker JP (2001) Supermolecular organization of photosystem II and its associated light-harvesting antenna in Arabidopsis thaliana. Eur J Biochem 268:6020–6028